24th COBEM - 2017

24th ABCM International Congress of Mechanical Engineering
December 3-8, 2017, Curitiba, PR, Brazil

COBEM-2017-0476
DNS OF NON-NEWTONIAN GIESEKUS FLUID FLOW STABILITY

Analice Costacurta Brandi
Laison Junio da Silva Furlan
Faculdade de Ciências e Tecnologia, Universidade Estadual Paulista "Júlio de Mesquita Filho"
Rua Roberto Simonsen, 305
19060-900, Presidente Prudente - SP
analice@fct.unesp.br, laisonfurlan@gmail.com

Márcio Teixeira de Mendonça
Instituto de Aeronáutica e Espaço, Divisão de Propulsão Aeronáutica - CTA/IAE/APA
Pç Marechal Eduardo Gomes, 50
12228-904, São José dos Campos, SP
marciomtm@iae.cta.br

Arianne Alves da Silva
Matheus Tozo de Araujo
Leandro Franco de Souza
Instituto de Ciências Matemáticas e de Computação, Universidade de São Paulo
Av. Trabalhador São Carlense, 400
13566-590, São Carlos - SP
arianne@usp.br, matheustozo@gmail.com, lefraso@icmc.usp.br

Abstract. *Hydrodynamic instability has emerged as an active field of study in non-Newtonian fluid mechanics. The rising interest in this phenomenon originates mainly from its technological importance in the polymer industry. The flow of non-Newtonian fluids between parallel plates is a problem of considerable practical interest. In this paper, the stability of the non-stationary disturbances viscoelastic fluid is studied through the growth rate of Tollmien-Schlichting waves for incompressible Poiseuille flow. The mathematical model adopted for the non-Newtonian fluid stress tensor is the Giesekus. The analysis is carried out by means of Direct Numerical Simulation (DNS). In the DNS formulation, the Navier-Stokes equations along with the Giesekus constitutive equation are solved using high-order finite differences numerical model. Results are presented for the Oldroyd-B fluid and compared with the Giesekus fluid. The results show that the amplification rates obtained differ from the Newtonian fluid as the α values increase. Comparisons are presented considering the maximum amplification rates for Newtonian and non-Newtonian fluid for different values of the Reynolds number, Weissenberg number and mobility parameter.*

Keywords: *laminar-turbulent transition, Giesekus fluid, Poiseuille flow, Direct Numerical Simulation*

1. INTRODUCTION

Non-Newtonian fluids are fluids where the relation between stress and strain is not linear and the viscosity depends on the shear rate. They are found in many industrial applications such as in the food and oil industries, paints and in cosmetic products. Blood is also a non-Newtonian fluid and that has important implications in the development of medical equipments. Due to its importance in these and other applications, non-Newtonian fluid properties and flow characteristics have received considerable attention in the late years and several research areas in fluid dynamics are extending their studies to consider non-Newtonian behaviour. The present study considers two of these areas, the direct numerical simulation of non-Newtonian fluid flows and their stability characteristics. The objectives are both for the development of accurate numerical tools for the simulation of non-Newtonian fluids and for the characterization and understanding of non-Newtonian flow transition behaviour. The base flow chosen for the present study was the planar Poiseuille flow, which is a well known benchmark flow problem in a simple topology that allow the investigation to concentrate on the numerical and physical aspects of the research.

A stability analysis of planar Poiseuille flow of a non-Newtonian fluid was performed by Porteous and Denn in 1972 (Porteous and Denn, 1972a,b). The viscoelastic fluid models of a second-order fluid and a Maxwell fluid were investigated and a new elastic mode of the Orr-Sommerfeld equation was determined. Elasticity was found to be destabilizing for finite

disturbances. More recently, Palmer in 2007 has studied a one-dimensional planar channel. Two viscoelastic fluid models, the Giesekus and linear Phan-Thien Tanner (PTT) models, were investigated in one-, two- and three-layered flows and the eigenspectra were sought (Palmer, 2007).

In terms of numerical simulation, according to Sureshkumar *et al.* (1999), the linear stability analysis in complex viscoelastic fluid flows become extremely complicated by the hyperbolic nature of the constitutive differential equations. Furthermore, the presence of boundary layers of elastic tension require discretization methods capable of capturing abrupt changes in disturbed fields and require extremely fine mesh, becoming of high computational cost.

Recently, Zhang *et al.* (2013) has investigated the modal and non-modal stability of both FENE-P and Oldroyd-B fluids in channel flow. FENE-P includes an upper bound for the extension of polymer molecules and can more reliably represent dilute polymer solutions where significant drag reduction in the turbulent regime is observed. The stability analysis of the FENE-P Poiseuille flow in the inertia-dominated regime, $Re > 2000$ was investigated (Zhang *et al.*, 2013). The linear stability analyses of the FENE-P fluids have been performed by Arora and Khomami (Arora and Khomami, 2005) and very recently by Lieu *et al.* (Lieu *et al.*, 2013) on the inertialess regime of Couette flow. The Oldroyd-B fluid Poiseuille flow stability was also investigated usind DNS by Brandi *et al.* (Brandi *et al.*, 2015).

In this work, the investigation by Brandi *et al.* (Brandi *et al.*, 2015) on the stability of Oldroyd-B fluid flow in channels is extended to the class of non-Newtonian fluids known as Giesekus fluid. Direct numerical simulations are undertaken for a Poiseuille flow using the Giesekus constitutive equation.

For the numerical simulations the governing equations are written in a vorticity-velocity formulation. The linear system arising from the numerical solution of the Poisson equation is solved by a multigrid methods. The spatial derivatives are discretized by compact finite difference schemes. The time integration is carried out by a fourth-order Runge-Kutta method. In order to evaluate the maximum amplification rates, different values of dimensionless parameters are tested for Newtonian and non-Newtonian fluid flows.

2. MATHEMATICAL FORMULATION

The flow is assumed to be unsteady, non-Newtonian, two-dimensional and incompressible, withou body forces. The governing equations are the continuity and Navier-Stokes equations with a constitutive relation for the non-Newtonian extra-stress tensor, that in this work is considered the Giesekus constitutive equation. The basic conservation equations governing the flow are

$$\nabla \cdot \mathbf{u} = 0, \tag{1}$$

$$\rho \left(\frac{\partial \mathbf{u}}{\partial t} + \nabla \cdot (\mathbf{u}\mathbf{u}) \right) = -\nabla p + \nabla \cdot \mathbf{T}, \tag{2}$$

where $\mathbf{u}$ denotes the velocity field, t is the time, ρ is the fluid density, p is the pressure and $\mathbf{T}$ is the extra-stress tensor. In this paper we worked with viscoelastic flows governed by the non-linear Giesekus constitutive equation (Giesekus, 1982), that is given by

$$\mathbf{T} + \lambda \left(\overset{\nabla}{\mathbf{T}} + \frac{\alpha}{\eta_p} (\mathbf{T} \cdot \mathbf{T}) \right) = 2\eta_p \mathbf{D}, \tag{3}$$

where $\mathbf{D} = \frac{1}{2}(\nabla \mathbf{u} + (\nabla \mathbf{u})^T)$ is the rate of deformation tensor, λ is the relaxation-time of the fluid, α is the so-called mobility parameter, η_p is the polymer-contributed viscosity and $\overset{\nabla}{\mathbf{T}}$ is the upper-convected derivative of $\mathbf{T}$ defined by

$$\overset{\nabla}{\mathbf{T}} = \frac{\partial \mathbf{T}}{\partial t} + \nabla \cdot (\mathbf{u}\mathbf{T}) - \mathbf{T} \cdot (\nabla \mathbf{u})^T - (\nabla \mathbf{u}) \cdot \mathbf{T}.$$

Introducing the following non-dimensionalized scalings:

$$\mathbf{x}^* = \frac{x}{L}, \quad \mathbf{u}^* = \frac{\mathbf{u}}{U}, \quad t^* = \frac{U}{L} t, \quad p^* = \frac{p}{\rho U^2}, \quad \mathbf{T}^* = \frac{\mathbf{T}}{\rho U^2}, \tag{4}$$

where L and U denote length and velocity scales, respectively. These equations can then be written (omitting the symbol $*$ for convenience) as

$$\nabla \cdot \mathbf{u} = 0, \tag{5}$$

$$\frac{\partial \mathbf{u}}{\partial t} + \nabla \cdot (\mathbf{u}\mathbf{u}) = -\nabla p + \frac{\beta}{Re} \nabla^2 \mathbf{u} + \nabla \cdot \mathbf{T}, \tag{6}$$

$$\mathbf{T} + We \overset{\nabla}{\mathbf{T}} = 2 \frac{(1-\beta)}{Re} \mathbf{D}, \tag{7}$$

where the dimensionless parameters $Re = \dfrac{\rho U L}{\eta}$ and $Wi = \dfrac{\lambda U}{L}$ denote the associated Reynolds and Weissenberg numbers, respectively. The amount of Newtonian solvent is controlled by the dimensionless solvent viscosity coefficient, $\beta = \dfrac{\eta_s}{\eta_0}$, where $\eta_0 = \eta_s + \eta_p$ denotes the total shear viscosity; η_s and η_p represent the Newtonian solvent and polymeric viscosities, respectively.

2.1 Direct Numerical Simulation

The Direct Numerical Simulation (DNS) solves directly the Navier-Stokes equations, usually employing high order finite difference schemes, such that all scales of the flow are simulated, from the largest and most energetic to the smallest, without adding closing equations. The main restriction of this technique is related to the computational cost.

In order to eliminate the treatment of the pressure in the Navier-Stokes equations, we opted for the use of vorticity-velocity formulation. Thus, the vorticity in direction z, ω_z is defined by

$$\omega_z = \frac{\partial u}{\partial y} - \frac{\partial v}{\partial x}.$$

Therefore, the equations (5)–(7) in the two-dimensional and non-dimensional form can be rewritten as

$$\frac{\partial u}{\partial x} + \frac{\partial v}{\partial y} = 0, \tag{8}$$

$$\frac{\partial^2 v}{\partial x^2} + \frac{\partial^2 v}{\partial y^2} = -\frac{\partial \omega_z}{\partial x}, \tag{9}$$

$$\frac{\partial \omega_z}{\partial t} + \frac{\partial (u\omega_z)}{\partial x} + \frac{\partial (v\omega_z)}{\partial y} = \frac{\beta}{Re}\left(\frac{\partial^2 \omega_z}{\partial x^2} + \frac{\partial^2 \omega_z}{\partial y^2}\right) + \frac{\partial^2 T^{xx}}{\partial x \partial y} + \frac{\partial^2 T^{xy}}{\partial y^2} - \frac{\partial^2 T^{xy}}{\partial x^2} - \frac{\partial^2 T^{yy}}{\partial x \partial y}, \tag{10}$$

$$T^{xx} + Wi\Big(\frac{\partial T^{xx}}{\partial t} + \frac{\partial (uT^{xx})}{\partial x} + \frac{\partial (vT^{xx})}{\partial y} - 2T^{xx}\frac{\partial u}{\partial x} - 2T^{xy}\frac{\partial u}{\partial y}\Big) + \alpha\frac{WiRe}{(1-\beta)}(T^{xx^2} + T^{xy^2}) = \\ = 2\frac{(1-\beta)}{Re}\frac{\partial u}{\partial x}, \tag{11}$$

$$T^{xy} + Wi\Big(\frac{\partial T^{xy}}{\partial t} + \frac{\partial (uT^{xy})}{\partial x} + \frac{\partial (vT^{xy})}{\partial y} - T^{xx}\frac{\partial v}{\partial x} - T^{yy}\frac{\partial u}{\partial y}\Big) + \alpha\frac{WiRe}{(1-\beta)}(T^{xx}T^{xy} + T^{xy}T^{yy}) = \\ = \frac{(1-\beta)}{Re}\Big(\frac{\partial v}{\partial x} + \frac{\partial u}{\partial y}\Big), \tag{12}$$

$$T^{yy} + Wi\Big(\frac{\partial T^{yy}}{\partial t} + \frac{\partial (uT^{yy})}{\partial x} + \frac{\partial (vT^{yy})}{\partial y} - 2T^{xy}\frac{\partial v}{\partial x} - 2T^{yy}\frac{\partial v}{\partial y}\Big) + \alpha\frac{WiRe}{(1-\beta)}(T^{xy^2} + T^{yy^2}) = \\ = 2\frac{(1-\beta)}{Re}\frac{\partial v}{\partial y}. \tag{13}$$

In the plan Poiseuille flow of a viscoelastic fluid problem, represented in Fig. 1, there are three types of boundary conditions used: inflow, outflow and wall boundary conditions. The inflow is specified according to the following conditions

$$u = U(y), \quad v = 0 \quad \text{and} \quad \mathbf{T} = 0. \tag{14}$$

On wall boundaries, the no-slip condition and impermeability $(u = 0, v = 0)$ are employed. At the outflow homogeneous Neumann condition are considered for both the velocity and the non-Newtonian contribution.

2.2 Base flow

In this paper we study viscoelastic plane Poiseuille flow where x and y represent the streamwise and wall-normal directions. To calculate the base flow, it is assumed that all variables are dependent only on the y axis, except for the pressure whose gradient is constant in the x direction. Assume that in the y direction the domain extends from $y = -1$ to $y = 1$.

For the Giesekus fluid the base flow was generated numerically by two-dimensional DNS code, without disturbances, and the simulations performed until the flow reached the steady state. Also, the variables for the base flow were taken in

the middle of the channel. For Oldroyd-B fluid the streamwise velocity component of the base flow coincides with the Poiseuille parabolic solution given by the function $u = 1 - y^2$. In addition, the wall-normal velocity, the vorticity and the non-Newtonian tensor components are given by

$$v = 0, \qquad \omega_z = -2y, \qquad T^{xx} = 8y^2 Wi \frac{(1-\beta)}{Re}, \qquad T^{xy} = 2y \frac{(\beta - 1)}{Re}, \qquad T^{yy} = 0. \tag{15}$$

3. NUMERICAL METHOD

The system of equations (5)–(7) is solved numerically in the domain as shown in Fig. 1. The calculations are done on an orthogonal uniform grid, parallel to the wall. The fluid enters the computational domain at $x = x_0$ and exits at the outflow boundary $x = x_{max}$. In this work, the behavior of infinitesimal disturbances in the flow is investigated. Steady disturbances are introduced into the flow field using suction and blowing of mass at a disturbance strip on the walls (Fasel *et al.*, 1990). This strip is located between x_1 and x_2.

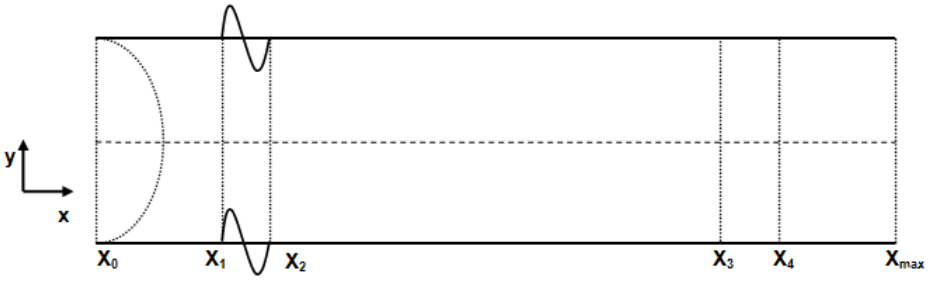

Figure 1. Definition of the computational domain for 2D Poiseuille flow.

At the beginning, time $t = 0$, the flow is undisturbed, therefore from time $t > 0$, the disturbances are introduced in a disturbance strip near the inflow, through the imposition of the v velocity:

$$v = Af(x)\, sin(\omega_t\, t), \quad x_1 < x < x_2, \tag{16}$$

and

$$v = 0, \quad x \leq x_1 \quad \text{or} \quad x \geq x_2, \tag{17}$$

where A is a constant used to adjust the amplitude of the disturbances, $f(x)$ is a 9th-order function, ω_t is the disturbance temporal frequency and the points x_1 and x_2 are the initial and the last point of the disturbance strip. The values of $f(x)$, its first, and second derivatives are zero in these extreme points. In the region located between x_0 and x_1 and x_3 and x_4 a buffer domain technique, from (Kloker *et al.*, 1993), is implemented in order to avoid wave reflections from the inflow and outflow boundaries, respectively.

The time derivatives in the vorticity transport and the components of the non-Newtonian extra-stress tensor equations are discretized with a classical four step fourth-order Runge-Kutta integration scheme (Ferziger and Peric, 1997). The spatial derivatives are calculated using a high-order compact finite difference-schemes (Souza *et al.*, 2005; Souza, 2003; Lele, 1992; Kloker, 1998). The use of the adopted compact finite differences to estimate the first and second spatial derivatives requires the solution of tridiagonal linear systems. The numerical derivative approximations have 5th- and 6th-order of accuracy (Souza *et al.*, 2005). The Poisson equation is solved using a multigrid Full Approximation Scheme (FAS) (Stüben and Trottenberg, 1981).

Finally, with the purpose of eliminating numerical (spurious) oscillations, a filter is applied after the last Runge-Kutta step. The filter adopted requires the solution of a pentadiagonal system. This filter is applied in the vorticity component in the streamwise direction and in the non-Newtonian extra-stress tensor components.

We solve Eqs. (8)–(13) numerically by the application of the following algorithm:
Step 1: Apply a step of the time integrator for the vorticity and the non-Newtonian extra-stress tensor.
Step 2: Apply the functions responsible for the damping and relaminarization zones.
Step 3: Introduce the disturbances by suction and blowing at the walls.
Step 4: Calculate the right hand side of Eq. (9).
Step 5: Calculate the v velocity by solving the Poisson equation [Eq. (9)].
Step 6: Calculate the value of u velocity through Eq. (8).

Step 7: Calculate the ω_z vorticity through Eq. (10).
Step 8: Calculate the components of the non-Newtonian extra-stress tensor through Eqs. (11)–(13).
Step 9: Update the vorticity value ω_z and the components of the non-Newtonian extra-stress tensor at the walls.
Step 10: Apply the filter after the last sub-step of the time integrator.

The numerical simulation finishes when the desired wall clock time is reached.

4. NUMERICAL RESULTS

In this section, stability analysis of the two-dimensional flow between two parallel plates for viscoelastic fluid of Giesekus type is presented. This paper present comparisons between the present results with Giesekus fluid and the results for the Olroyd-B fluid, in order to verify the numerical code. In addition, the influence of the α parameter on the Giesekus type viscoelastic flow simulation was analyzed.

4.1 Code Verification

In order to verify the actual DNS code implemented with the Giesekus fluid, we consider the plane Poiseuille flow between two parallel plates. Numerical simulations were performed in order to compare the base flow generated numerically with the DNS code implemented with the Giesekus model, considering $\alpha = 0$ in mathematical model and comparing with the base flow generated analytically (Eq. (15)) with the DNS code implemented with the Oldroyd-B model.

For verification test of implemented code, the following parameters were adopted: the number of points in the streamwise and wall-normal directions are $i_{max} = 729$ and $j_{max} = 129$, respectively; the distance between two consecutive points in the x- and y-directions are $dx = 2\pi/(32\alpha_r)$ and $dy = 2/(jmax - 1)$, respectively, where α_r is the real part of the wavenumber; the time steps per wave period is 128.

Figure 2 shows the development of the maximum disturbance velocity u_{max} in the streamwise direction (x) obtained by time Fourier analysis simulated with Oldroyd-B and Giesekus models. In this figure the Weissenberg number and the constant β were fixed to $Wi = 1.0$ and $\beta = 0.25$ and the varied Reynolds number. It can be seem that the two models are in agreement.

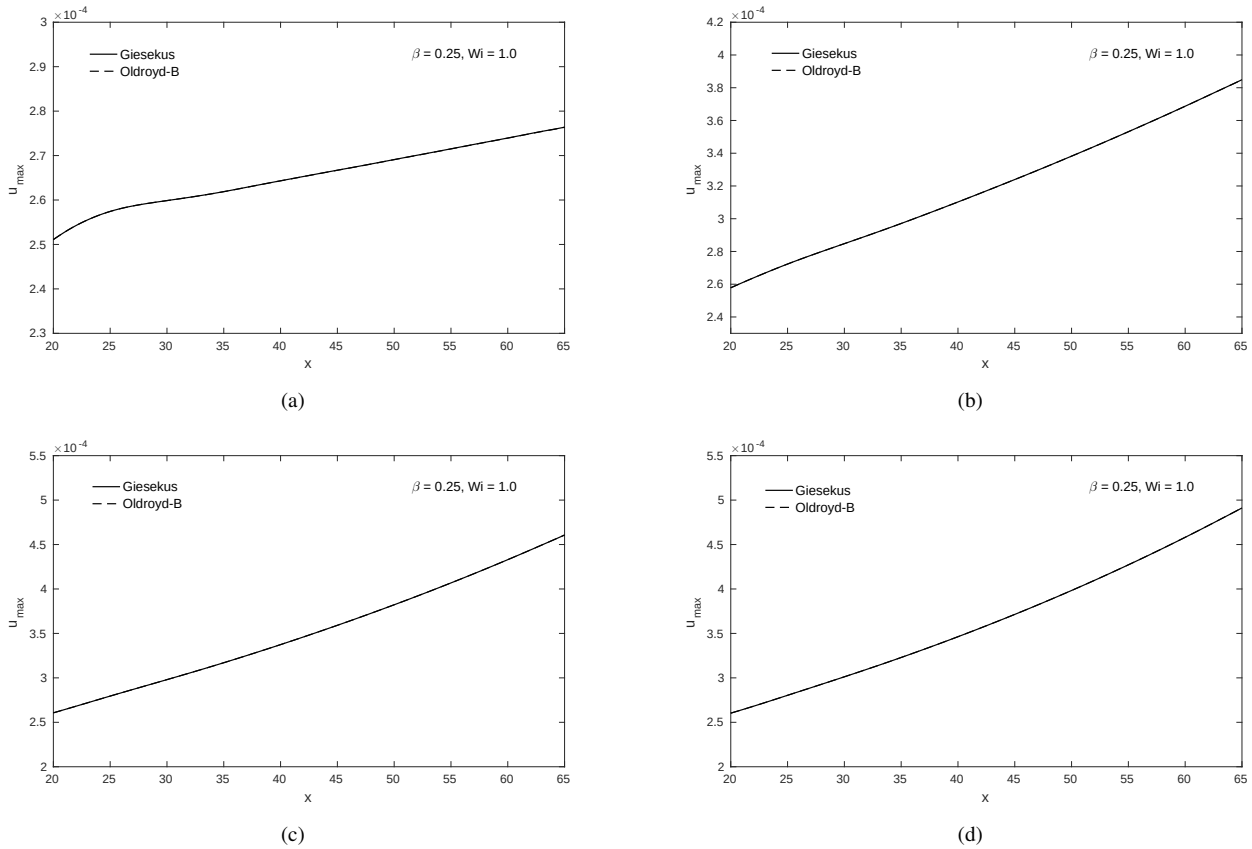

Figure 2. Maximum streamwise velocity disturbance development in the streamwise direction for different Reynolds values. a) $Re = 5000$, b) $Re = 6000$, c) $Re = 7000$ and d) $Re = 8000$.

Other cases with different β, Reynolds and Weissenberg values are performed and shown in Figs 3 and 4 to verify the

behavior of T^{xx} and T^{xy} non-Newtonian tensors. These results shows that the two models are in agreement also to the non-Newtonian tensors.

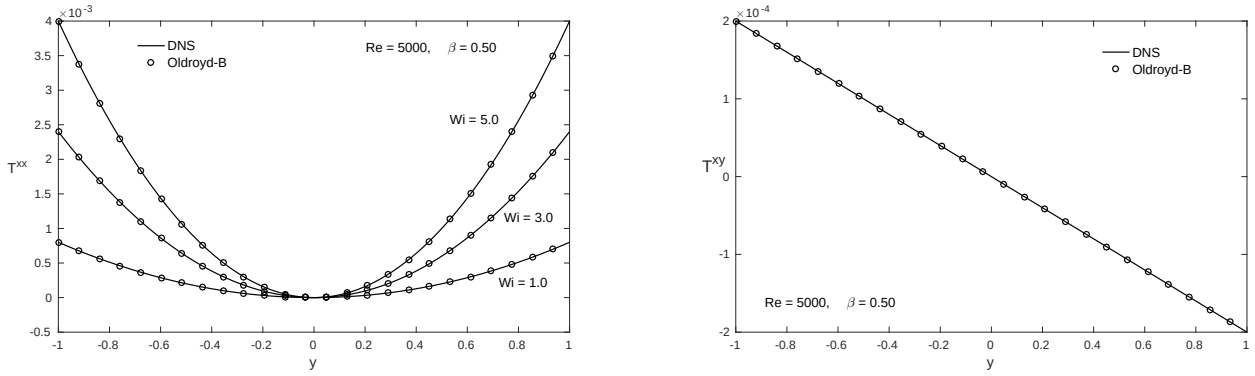

(a) (b)

Figure 3. Numerical solutions obtained at the middle of the channel of Giesekus and Oldroyd-B fluids flows using different parameters.

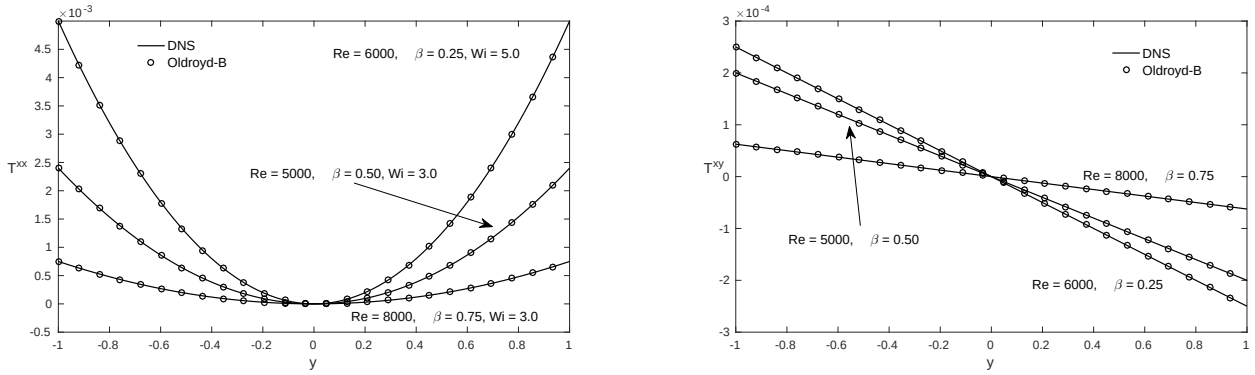

(a) (b)

Figure 4. Numerical solutions obtained at the middle of the channel of Giesekus and Oldroyd-B fluids flows using different parameters.

4.2 The α Variation – Giesekus Model

In order to evaluate the maximum amplification rates, different numerical simulations were performed by varying the non-dimensional parameters for the viscoelastic fluid. Considering the viscoelastic Poiseuille flow, using the Giesekus model, the effect of the alpha parameter in the numerical simulations were analyzed.

In these simulations three different Reynolds values were considered: Re = 5000, 6000 and 7000, three different values of α: α = 0.25, 0.5 and 0.75, two different Weissenberg values: $Wi = 1.0$ and 10.0 and fixed $\beta = 0.75$.

The parameters adopted in the simulations carried out here were: the number of points in the streamwise and wall-normal directions are $i_{max} = 729$ and $j_{max} = 129$, respectively; the distance between two consecutive points in the x- and y-directions are $dx = 2\pi/(32\alpha_r)$ and $dy = 2/(jmax - 1)$, respectively, where α_r is the real part of the wavenumber; the time steps per wave period is 128, disturbance frequency $\omega_t = 0.27$. The parameter A to adjust the amplitude of the Tollmien-Schlichting waves was 1×10^{-4}.

Figures 5, 6 and 7 show the development of Tollmien-Schlichting waves for different dimensionless parameters in numerical simulations. In this figures the Weissenberg number were fixed to $Wi = 1.0$ and $Wi = 10.0$.

Figures 5(a) and 6(a) show that increasing α de flow becomes more unstable, or in other words for 5(a) the flow becomes less stable with increasing α. Figure 7(a) shows that increasing α the flow becomes more and more stable. Figures 5(b), 6(b) and 7(b) for $Wi = 10$, all show that the flow becomes more unstable with increasing α, regardless of the Reynolds number.

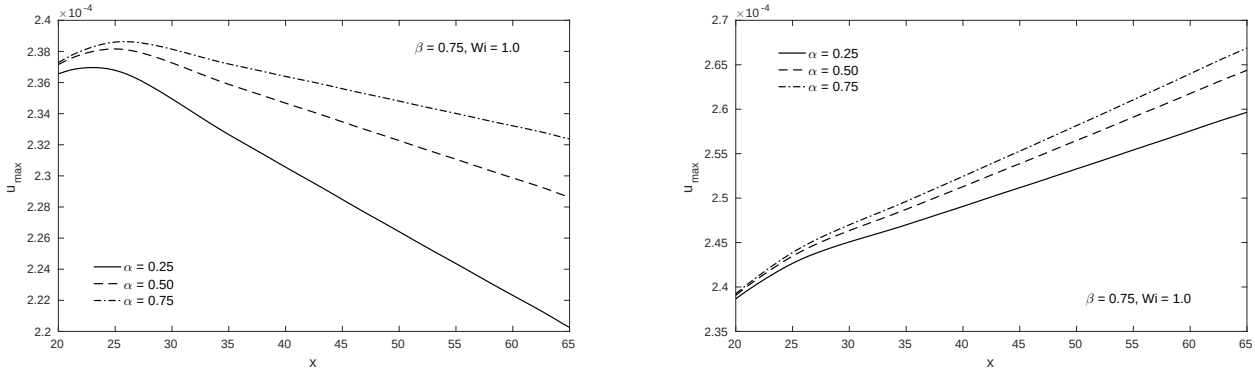

(a) (b)

Figure 5. Maximum streamwise velocity disturbance development in the streamwise direction for different α values. Fixed constant $\beta = 0.75$ and $Re = 5000$. a) $Wi = 1.0$ and b) $Wi = 10.0$.

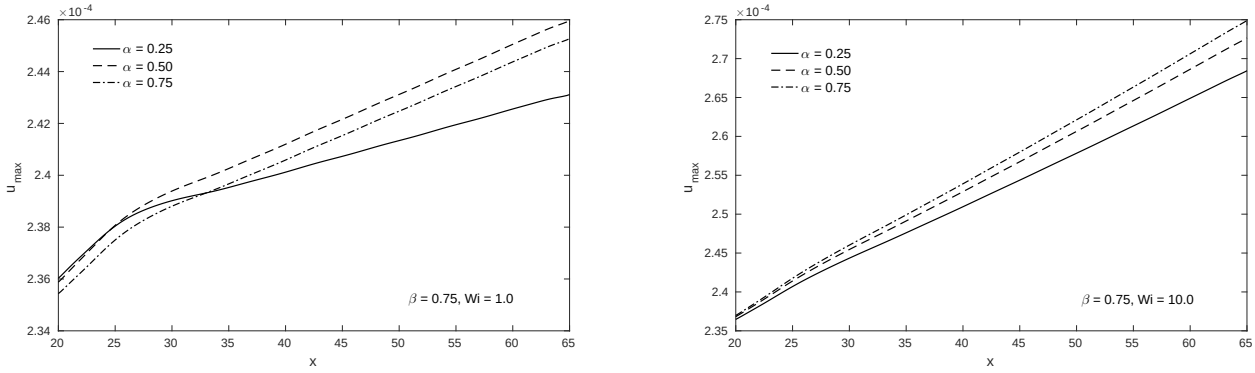

(a) (b)

Figure 6. Maximum streamwise velocity disturbance development in the streamwise direction for different α values. Fixed constant $\beta = 0.75$ and $Re = 6000$. a) $Wi = 1.0$ and b) $Wi = 10.0$.

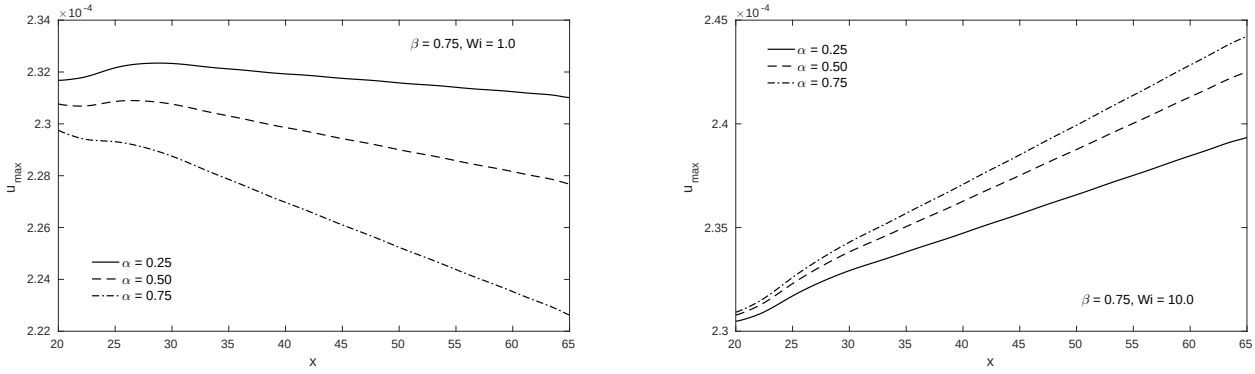

(a) (b)

Figure 7. Maximum streamwise velocity disturbance development in the streamwise direction for different α values. Fixed constant $\beta = 0.75$ and $Re = 7000$. a) $Wi = 1.0$ and b) $Wi = 10.0$.

5. CONCLUSIONS

The present paper presents a Direct Numerical Simulation to investigate of the Tollmien-Schlichting waves convection in a plane Poiseuille flow. For this numerical simulation of two-dimensional viscoelastic fluid flow using the Giesekus constitutive equation was carried out. The governing equations are written in a vorticity-velocity formulation. In order to evaluate the maximum amplification rates for different α values, different values of dimensionless parameters are tested for Newtonian and non-Newtonian fluid flows.

The results show that for most of the cases considered, the flow becomes more unstable with increasing α, but for high Reynolds number and low Weissenberg number the flow becomes more and more stable with increasing alpha.

6. ACKNOWLEDGEMENTS

This work was supported by Fundação de Amparo à Pesquisa do Estado de São Paulo (FAPESP) under Grant No. 2017/11068-6.

7. REFERENCES

Arora, K. and Khomami, B., 2005. "The influence of finite extensibility on the eigenspectrum of dilute polymeric solutions". *Journal of Non-Newtonian Fluid Mechanics*, Vol. 129, pp. 56–60.

Brandi, A.C., Gervazoni, E.S., Mendonca, M.T. and Souza, L.F., 2015. "Influence of elastic forces in transition phenomeon". In *Proceedings of the 23rd International Congress of Mechanical Engineering - COBEM2015*. Rio de Janeiro, RJ.

Fasel, H.F., Rist, U. and Konzelmann, U., 1990. "Numerical investigation of the three-dimensional development in boundary-layer transition". *AIAA*, Vol. **28**, pp. 29–37.

Ferziger, J.H. and Peric, M., 1997. *Computational Methods for Fluid Dynamics*. Springer-Verlag Berlin Heidelberg New York.

Giesekus, H., 1982. "A simple constitutive equation for polymer fluids based on the concept of deformation-dependent tensorial mobility". *Journal of Non-Newtonian Fluid Mechanics*, Vol. 11, pp. 69–109.

Kloker, M., 1998. "A robust high-resolution split-type compact fd scheme for spatial direct numerical simulation of boundary-layer transition". *Applied Scientific Research*, Vol. **59**, pp. 353–377.

Kloker, M., Konzelmann, U. and Fasel, H.F., 1993. "Outflow boundary conditions for spatial navier-stokes simulations of transition boundary layers". *AIAA Journal*, Vol. **31**, pp. 620–628.

Lele, S., 1992. "Compact finite difference schemes with spectral-like resolution". *J. Comput. Phys.*, Vol. **103**, pp. 16–42.

Lieu, B.K., Jovanovic, M.R. and KUMAR, S., 2013. "Worst-case amplification of disturbances in inertialess couette flow of viscoelastic fluids". *Journal of Fluid Mechanics*, Vol. 723, pp. 232–263.

Palmer, A., 2007. *Linear Stability Analyses of Poiseuille Flows of Viscoelastic Liquids*. Ph.D. thesis, The University of Wales, Aberystwyth, United Kingdom.

Porteous, K.C. and Denn, M.M., 1972a. "Linear stability of plane poiseuille flow of viscoelastic liquids". *Transactions of The Society of Rheology*, Vol. 16, pp. 295–308.

Porteous, K.C. and Denn, M.M., 1972b. "Nonlinear stability of plane poiseuille flow of viscoelastic liquids". *Transactions of The Society of Rheology*, Vol. 16, pp. 309–319.

Souza, L.F., 2003. *Instabilidade Centrífuga e transição para turbulência em Escoamentos Laminares Sobre Superfícies Côncavas*. Ph.D. thesis, Instituto Tecnológico de Aeronáutica.

Souza, L.F., Mendonça, M.T. and Medeiros, M.A.F., 2005. "The advantages of using high-order finite differences schemes in laminar-turbulent transition studies". *International Journal for Numerical Methods in Fluids*, Vol. **48**, pp. 565–592.

Stüben, K. and Trottenberg, U., 1981. *Nonlinear multigrid methods, the full approximation scheme*, Köln-Porz, chapter 5, pp. 58–71.

Sureshkumar, R., Smith, M.D., Armstrong, R.C. and Brown, R.A., 1999. "Linear stability and dynamics of viscoelastic flows using time-dependent numerical simulations". *Journal of Non-Newtonian Fluid Mechanics*, Vol. 82, pp. 57–104.

Zhang, M., Lashgari, I., Zaki, T.A. and Brandt, L., 2013. "Linear stability analysis of channel flow of viscoelastic oldroyd-b and fene-p fluids". *Journal of Fluid Mechanics*, Vol. 737, pp. 249–279.

8. RESPONSIBILITY NOTICE

The authors are the only responsible for the printed material included in this paper.